# Author's Accepted Manuscript

Uncoupled poroelastic and intrinsic viscoelastic dissipation in cartilage

Guebum Han, Cole Hess, Melih Eriten, Corinne R. Henak



www.elsevier.com/locate/imbbm

PII: S1751-6161(18)30150-4

DOI: https://doi.org/10.1016/j.jmbbm.2018.04.024

**JMBBM2775** Reference:

To appear in: Journal of the Mechanical Behavior of Biomedical Materials

Received date: 14 February 2018 Revised date: 9 April 2018 Accepted date: 25 April 2018

Cite this article as: Guebum Han, Cole Hess, Melih Eriten and Corinne R. Henak, Uncoupled poroelastic and intrinsic viscoelastic dissipation in cartilage, Mechanical Biomedical of the **Behavior** of Materials. https://doi.org/10.1016/j.jmbbm.2018.04.024

This is a PDF file of an unedited manuscript that has been accepted for publication. As a service to our customers we are providing this early version of the manuscript. The manuscript will undergo copyediting, typesetting, and review of the resulting galley proof before it is published in its final citable form. Please note that during the production process errors may be discovered which could affect the content, and all legal disclaimers that apply to the journal pertain.

# Uncoupled poroelastic and intrinsic viscoelastic dissipation in cartilage

### **First Revision**

Guebum Han <sup>a</sup>, Cole Hess <sup>a</sup>, Melih Eriten <sup>a</sup>, and Corinne R. Henak <sup>a,b,\*</sup>

<sup>a</sup>Department of Mechanical Engineering, University of Wisconsin-Madison, 1513 University Ave, Madison, Wisconsin 53706, USA

<sup>b</sup>Department of Biomedical Engineering, University of Wisconsin-Madison, 1550 University Ave, Madison, Wisconsin 53706, USA

\*Corresponding author

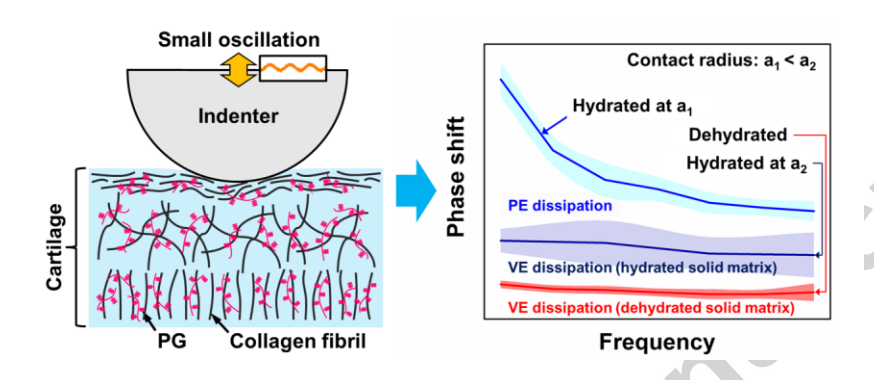
E-mail: ghan28@wisc.edu (G. Han), cole.hess@wisc.edu (C. Hess), eriten@wisc.edu (M. Eriten), chenak@wisc.edu (C.R. Henak)

### **Abstract**

This paper studies uncoupled poroelastic (flow-dependent) and intrinsic viscoelastic (flow-independent) energy dissipation mechanisms via their dependence on characteristic lengths to understand the root of cartilage's broadband dissipation behavior. Phase shift and dynamic modulus were measured from dynamic microindentation tests conducted on hydrated cartilage at different contact radii, as well as on dehydrated cartilage. Cartilage weight and thickness were recorded during dehydration. Phase shifts revealed poroelastic- and viscoelastic-dominant dissipation regimes in hydrated cartilage. Specifically, phase shift at a relatively small radius was governed by poroviscoelasticity, while phase shift at a relatively large radius was dominantly governed by intrinsic viscoelasticity. The uncoupled dissipation mechanisms demonstrated that intrinsic viscoelastic dissipation provided sustained broadband dissipation for all length scales, and additional poroelastic dissipation increased total dissipation at small length scales. Dehydration decreased intrinsic viscoelastic dissipation of cartilage. The findings demonstrated a possibility to measure poroelastic and intrinsic viscoelastic properties of cartilage at similar

microscale lengths. Also they encouraged development of broadband cartilage like-dampers and provided important design parameters to maximize their performance.

### **Graphical Abstract**



### **Keywords**

Articular cartilage; poroelasticity; intrinsic viscoelasticity; energy dissipation; broadband properties

### 1. Introduction

Articular cartilage is a connective tissue that functions as a load-bearing and dissipative material over a broadband spectrum of loading frequency. Cartilage has a heterogeneous structure composed of the dense solid matrix (e.g., collagen fibrils and proteoglycans) and fluid (Mow et al., 1992). Fluid is the largest constituent (about 60 - 85 % of wet weight), and it plays an important role in swelling interfibriliar space (about 30 % of total water) and extrafibriliar space (Maroudas et al., 1991; Mow et al., 1992; Torzilli, 1985). Cartilage dehydrate and rehydrate due to pressure-induced exudation of fluid through the solid matrix under normal loading conditions *in vivo*. Time-dependent properties of cartilage are from coupled mechanisms of the solid matrix and fluid flow. The mechanisms have been characterized as poroelasticity and intrinsic

viscoelasticity, resulting in efficient and sustained broadband dissipative properties (Nia et al., 2011; Nia et al., 2013; Fulcher et al., 2009; Lawless et al., 2017).

Previous studies have provided evidence on poroelasticity and intrinsic viscoelasticity of cartilage, but the relative contributions of the two are unclear. Poroelasticity-driven dissipation and response originates from solid-fluid frictional (viscous drag) interaction, and therefore is flow-dependent (Nia et al., 2011; Nia et al., 2015). Previous studies showed that poroelasticitydriven dissipation was dominant at relatively small length scales (about 5-6 um) under oscillatory loading (Nia et al., 2011; Nia et al., 2013). Intrinsic viscoelasticity-driven dissipation is associated with delay due to molecular friction and rearrangement of a solid matrix (Nia et al., 2011; Nia et al., 2015), and therefore is flow-independent (June et al., 2009; Lai and Hu, 2017; Mak, 1986). Previous work measured intrinsic viscoelasticity of cartilage by employing macroscale compression tests (Fulcher et al., 2009; June et al., 2009; Lawless et al., 2017; Mak, 1986) and small magnitude shear loading (Henak et al., 2016). Although a few studies have individually measured poroelasticity (Nia et al., 2011; Nia et al., 2013) and intrinsic viscoelasticity of cartilage (Fulcher et al., 2009; Lawless et al., 2017) over a wide spectrum of frequency, their relative contributions have not been uncoupled from each other. Also, it is difficult to utilize previously reported results to uncouple the mechanisms because test length scales (about 5-6 µm for poroelasticity (local) versus about 5 mm for intrinsic viscoelasticity (full-thickness)) are polarized, and therefore depth-dependent heterogeneous structure (e.g., collagen direction and diameter) of cartilage cannot be compared precisely.

Poroelasticity-driven dissipation is length-dependent, while intrinsic viscoelasticity-driven dissipation is not. This difference provides a means to distinguish the contributions of the two. Poroelastic dissipation is flow-dependent, and therefore is associated with characteristic poroelastic diffusion time. The diffusion time is proportional to the squared of a characteristic length (e.g., contact radius) (Lai and Hu, 2017; Nia et al., 2011). Consequently, a characteristic length can govern poroelasticity-driven dissipation. A poroelasticity-driven dissipation spectrum

moves toward a low frequency range as a characteristic length increases, and its peak frequency,  $f_{poro}$ , can be estimated with poroelastic diffusion time (Figure 1) (Lai and Hu, 2017; Nia et al., 2011). In contrast, intrinsic viscoelastic dissipation is flow-independent (June et al., 2009; Lai and Hu, 2017; Mak, 1986). Accordingly, an intrinsic viscoelasticity-driven dissipation spectrum and its peak frequency,  $f_{visco}$ , are independent of a characteristic length (Figure 1). Consequently, the two dissipation mechanisms can be distinguished over a broad frequency range by carefully selecting characteristic lengths.

The main aim of this study is to understand the origin of cartilage's broadband dissipation behavior by uncoupling the poroelastic and intrinsic viscoelastic dissipation mechanisms through their dependence on characteristic lengths. Phase shifts, a measure of dissipation, were measured at three different contact radii (characteristic lengths). Results of phase shifts were compared to uncouple the dissipation mechanisms. Dynamic moduli were also measured to examine dynamic response of cartilage based on the uncoupled dissipation mechanisms. In addition, phase shift and dynamic modulus of dehydrated cartilage were measured to further investigate the effect of fluid loss on broadband dissipative and mechanical properties.

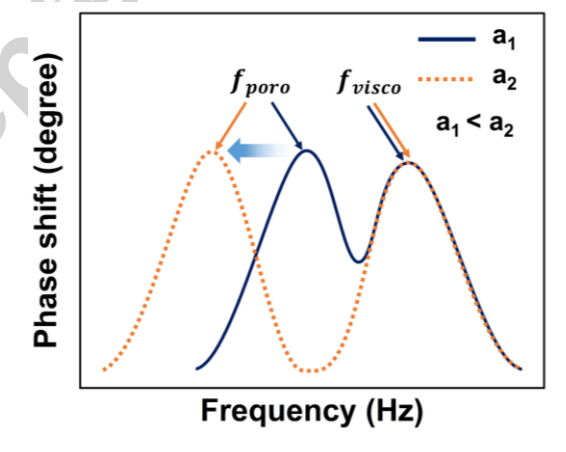


Figure 1 Schematic diagram of dependence of poroelastic and intrinsic viscoelastic energy dissipation on contact radii. The poroelastic peak frequency,  $f_{poro}$ , is inversely proportional to the square of the contact radius, a (Eq. 5). Therefore, the effects of the two mechanisms can be uncoupled by performing dynamic testing at different contact radii.

### 2. Methods

### 2.1 Sample Preparation

Full-thickness cartilage samples were harvested from patellae of porcine joints (12 animals, 5-6 months old, gender unknown and assumed random). Cylindrical samples with a diameter of 6 mm were obtained using a biopsy punch and a scalpel. Subchondral bone was trimmed using a microtome to create a level articular surface for indentation testing. The deep zone of each sample was adhered to the center of a glass petri dish (Loctite 495, Henkel, Germany). Dulbecco's phosphate-buffered saline (DPBS) was used to keep samples hydrated during preparation.

### 2.2 Dehydration curve of cartilage

Dehydration of cartilage was evaluated to determine how long to dehydrate cartilage for testing. Samples were dehydrated at room temperature of 20.9 °C and relative humidity of 25 %. The weight of cartilage was measured every 10 minutes for 3 hours using an analytical electronic balance (MS104TS, Mettler Toledo, OH). After 3 hours, the weight of cartilage was measured every 20 minutes until 4 hours of dehydration, and then the weight was measured at 5 hours. The thickness of cartilage was also measured every 45 minutes using a digital caliper before 2 hours of dehydration. After 2 hours, the thickness was measured every hour until 5 hours of dehydration. The measured weight and thickness of cartilage during dehydration were normalized with the initial weight and thickness. A total of three samples were tested, they were from one patella.

### 2.3 Broadband Dynamic Indentation Tests

Dynamic microindentation tests were conducted to measure phase shift and dynamic modulus, in order to uncouple poroelastic and viscoelastic effects. Tests were conducted on a Hysitron TI950 TriboIndenter (Bruker Inc, Minneapolis, MN) using a diamond sphero-conical indenter with a tip radius of 50 μm and cone semi-angle of 45°, and a sapphire spherical indenter with a tip radius of 1 mm. For each test, a static displacement was applied and held until equilibrium, then a small amplitude (0.5-2 nm) frequency sweep was applied. Open-loop control setting was used, resulting

in curves similar to force-relaxation curves for hydrated cartilage (Figure 2b) and curves similar to creep curves for dehydrated cartilage. A slight drift in force measurement was observed, likely from thermal drift (Lai and Hu, 2017). A reference frequency technique was employed to minimize the effect of the drift by correcting contact area based on measured stiffness at a reference frequency (Hysitron, 2014). A 220 Hz reference frequency was imposed between test frequencies.

Contact radii were adjusted by changing the indenter or the static displacement (Figure 2). Equilibrium time and frequencies tested varied as a function of the contact radius. Hydrated cartilage was tested with three contact radii, and was kept hydrated with DPBS during tests. The smallest contact radius,  $a_{small} = 13.21 \pm 0.59 \,\mu\text{m}$ , was achieved with the 50  $\mu$ m radius spheroconical indenter, held at a static displacement of  $3.50 \pm 0.32 \,\mu m$  for 20 seconds, followed by a frequency sweep from 5 Hz to 100 Hz in 7 randomized segments (contact area: 549.20 ± 49.52  $\mu$ m<sup>2</sup>). The middle contact radius,  $a_{medium} = 32.77 \pm 0.77 \,\mu$ m, was achieved with the 1 mm radius tip, held at a static displacement of  $1.07 \pm 0.05 \,\mu m$  for 40 seconds, followed by a frequency sweep from 5 Hz to 100 Hz in 4 randomized segments (contact area: 3375.43 + 158.20  $\mu$ m<sup>2</sup>). The largest contact radius,  $a_{large} = 43.13 \pm 0.85 \,\mu$ m, was achieved with the 1 mm radius tip, held at a static displacement of  $1.86 \pm 0.07 \,\mu m$  for 100 seconds, followed by a frequency sweep in 4 randomized segments from 25 Hz to 100 Hz (contact area: 5846.20  $\pm$ 229.21 µm<sup>2</sup>). A low frequency of 5 Hz had to be sacrificed due to limitations in the number of data acquisition points coupled with the long time for equilibrium. Dynamic indentation tests were performed on dehydrated cartilage with a single indenter (tip radius of 50 μm) because no flow-dependent effects were expected. Cartilage was dehydrated for 5 hours in the condition used for obtaining the dehydration curves; 5 hours were determined based on the curves. The tip was indented, held a static displacement of  $0.68 \pm 0.14 \, \mu m$  for 20 seconds, resulting in a contact radius of  $5.79 \pm 0.60 \,\mu$  m (contact area:  $103.19 \pm 23.94 \,\mu$ m<sup>2</sup>). Following the 20 second

equilibrium, a frequency sweep from 5 Hz to 100 Hz (7 segments, randomized) was implemented. For all tests, displacements and contact radii were estimated at about 10 seconds before the end of tests. Contact radii, *a*, were estimated by using Hertzian contact theory (Hertz, 1881):

$$a = \sqrt{R\delta_{static}}$$
 (1)

where R is the indenter radius and  $\delta_{static}$  is the static displacement (Figure 2). Each testing configuration - hydrated at three radii and dehydrated - was tested at three locations on three samples. Each sample was from different patella, taken from two animals. Test locations were selected near the center of samples to avoid the effect of edge on measurement results.

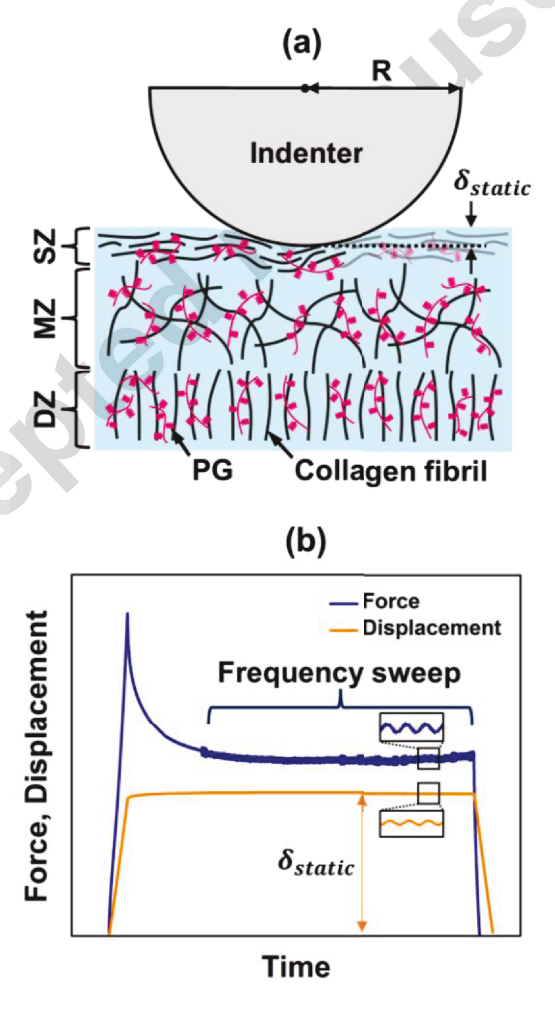


Figure 2 (a) Schematic diagram of contact between impermeable indenter and cartilage and (b) representatives of force-time and displacement-time curves from hydrated cartilage. R

and  $\delta_{static}$  are the tip radius and the static displacement, respectively. SZ, MZ, and DZ are superficial zone, middle zone, and deep zone, respectively. Since  $\delta_{static}$  (about 1-3 µm) was shallow, the measured values were from SZ (10-20% of total thickness (Mow et al., 1992) = about 300 µm).

# 2.4 Estimation of poroelastic peak frequency from force relaxation curve

The poroelastic peak frequency,  $f_{poro}$ , was estimated to check if the experimentally-measured trend of phase shift versus frequency was consistent with the theoretical peak. This information was used as secondary confirmation of poroelastic dominant dissipation. To estimate  $f_{poro}$ , diffusivity, D, of hydrated cartilage was obtained by fitting an experimental force relaxation curve to a master curve for a half-space poroelastic material under a spherical indenter (rigid, frictionless, and impermeable) (Hu et al., 2010). A portion of a force relaxation curve with a 50  $\mu$ m radius tip (before the dynamic load application) was used as F(t) because the displacement was constantly maintained even under an open-loop control setting. First, diffusion at time, t, was estimated as a length scale,  $I_{PE}$ , as follows (Hu et al., 2010):

$$l_{PE} = \sqrt{Dt}$$
 (2)

Next, an experimental force relaxation curve, F(t), was normalized into a dimensionless curve, g, by using  $l_{PE}$  and a at  $\delta_{static}$  as follows (Hu et al., 2010):

$$\frac{F(t) - F(\infty)}{F(0) - F(\infty)} = g\left(\frac{l_{PE}^2}{a^2}\right) = g\left(\frac{Dt}{a^2}\right) = g(\tau)$$
(3)

where F(0) and  $F(\infty)$  are the instantaneous force at time = 0 s and the equilibrium force at infinite time, respectively. F(0),  $F(\infty)$ , and D were fitting parameters, and they were initially guessed for the purpose of normalizing a force relaxation curve. The normalized dimensionless curve was fitted with the fitting parameters to a master curve (Hu et al., 2010):

$$g(\tau) = 0.491e^{-0.908\sqrt{\tau}} + 0.509e^{-1.679\tau}$$
(4)

As a result of the curve fitting, F(0),  $F(\infty)$ , and D were determined, allowing  $f_{poro}$  to be estimated (Lai and Hu, 2017; Nia et al., 2011):

$$f_{poro} \sim \frac{1}{\tau_{poro}} = \frac{D}{a^2} \tag{5}$$

where  $\tau_{poro}$  is the poroelastic time constant.

### 2.5 Statistical Analysis

The Kruskal-Wallis test was used to determine the statistical difference in phase shift and dynamic modulus among four test sets (hydrated cartilage at a<sub>small</sub>, a<sub>medium</sub>, and a<sub>large</sub>, and dehydrated cartilage). If a significant difference was found from the above step, the Mann-Whitney U test was used to identify the source of the significant difference by comparing two test sets. In addition, the Kruskal-Wallis test was used to determine the dependence of phase shift and dynamic modulus on frequency in each test set. All statistical analysis was conducted using MATLAB (The MathWorks, Inc., Natick, MA). A significance level of 5% was employed for all tests.

### 3. Results

Phase shifts of hydrated cartilage from  $a_{small}$  were significantly different from those from a large contact radius (i.e.,  $a_{medium}$  and  $a_{large}$ ) (p<0.05) (Figure 3a). Phase shift from  $a_{small}$  gradually decreased from 5 Hz to 100 Hz, and its dependence on frequency was significant (p<0.05). The maximum and minimum values were  $30.50 \pm 2.19$  degrees at 5 Hz and  $13.74 \pm 1.28$  degrees at 100 Hz, respectively. Phase shift from  $a_{medium}$  was steady over the frequency range, and it was not significantly frequency-dependent (p>0.05). The values at 5 Hz and 100 Hz were 9.97  $\pm$  1.50 degrees and  $8.16 \pm 2.87$  degrees, respectively. Phase shift from  $a_{medium}$  was lower than that from  $a_{small}$  over the frequency range (20.53 degrees at 5 Hz and 5.58 degrees at 100 Hz).

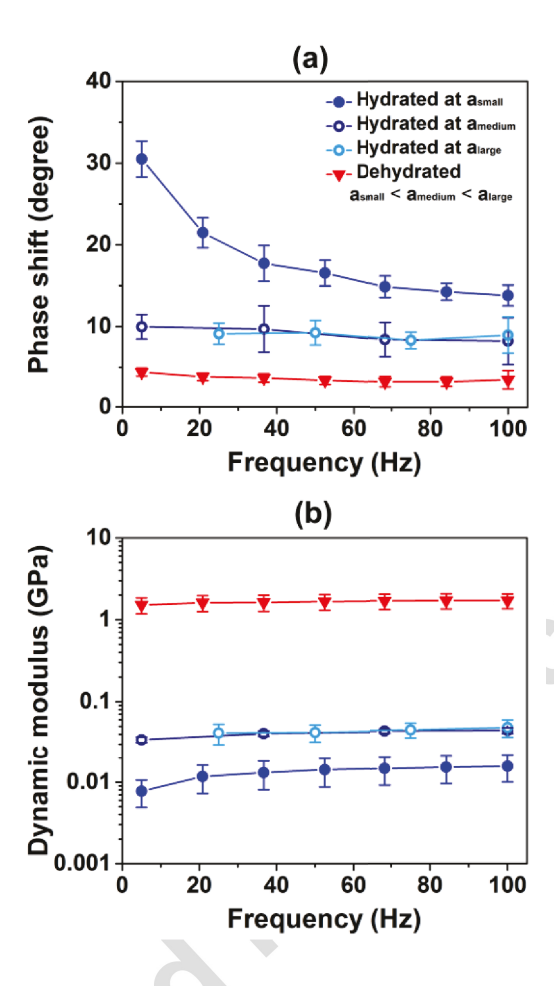


Figure 3 (a) Phase shifts and (b) dynamic moduli of hydrated and dehydrated cartilage. Error bars show standard deviation.

In contrast, phase shifts of hydrated cartilage from  $a_{medium}$  and  $a_{large}$  were not significantly different from each other (p>0.05). They were not dependent on frequency (p>0.05) (Figure 3a). Phase shifts from  $a_{large}$  were 9.12  $\pm$  1.29 degrees at 25 Hz and 8.89  $\pm$  2.22 degrees at 100 Hz.

Phase shift of dehydrated cartilage was significantly lower than phase shifts of hydrated cartilage (Figure 3a) (p<0.05). The phase shift at the dehydrated state was not dependent on frequency (4.42  $\pm$  0.49 degrees at 5 Hz and 3.41  $\pm$  1.13 degrees at 100 Hz) (p>0.05). Phase shift of dehydrated cartilage was approximately 3-7 times lower than that of hydrated cartilage.

Hydrated cartilage tested at  $a_{small}$  showed significantly lower dynamic modulus than that tested at a large contact radius (i.e.,  $a_{medium}$  and  $a_{large}$ ) (p<0.05), but dynamic moduli from  $a_{medium}$  and  $a_{large}$  were not significantly different (Figure 3b) (p>0.05). Dynamic modulus from  $a_{small}$ 

increased in a frequency-dependent manner from  $7.74 \pm 2.86$  MPa at 5 Hz to  $15.83 \pm 5.71$  MPa at 100 Hz (p<0.05). Dynamic modulus from  $a_{medium}$  slightly increased from  $34.07 \pm 2.68$  MPa at 5 Hz to  $43.18 \pm 3.47$  MPa at 100 Hz, and only the modulus at 5 Hz was significantly different than at any other frequencies (p<0.05). Dynamic modulus from  $a_{large}$  was not frequency-dependent (p>0.05), and the values at 25 Hz and 100 Hz were  $41.19 \pm 11.70$  MPa and  $47.00 \pm 11.33$  MPa. Although overall dynamic moduli at a large contact radius (i.e.,  $a_{medium}$  and  $a_{large}$ ) were significantly (p<0.05) higher than those at  $a_{small}$ , the relative increase with frequency was higher at  $a_{small}$ .

Dynamic modulus at the dehydrated state was significantly higher than that at the hydrated state (Figure 3b) (p<0.05). Dynamic modulus of dehydrated cartilage ranged from 1.51  $\pm$  0.33 GPa at 5 Hz to 1.70  $\pm$  0.35 GPa at 100 Hz, and it was not significantly dependent on frequency (p>0.05). Dynamic modulus at the dehydrated state was about 120 times and about 40 times higher than the overall dynamic moduli from  $a_{small}$  and a large contact radius (i.e.,  $a_{medium}$  and  $a_{large}$ ), respectively.

D was determined by fitting normalized force relaxation curves at  $a_{small}$  to the master curve (Eq. (3) and Eq. (4)). As a result, D was evaluated to be  $(3.89 \pm 1.64) \times 10^{-11}$  m<sup>2</sup>/s, and the R-squared value for the curve fitting was  $0.97 \pm 0.01$  (Figure 4). Furthermore,  $f_{poro}$  was estimated as  $0.22 \pm 0.09$  Hz by substituting the determined D into Eq. (5).

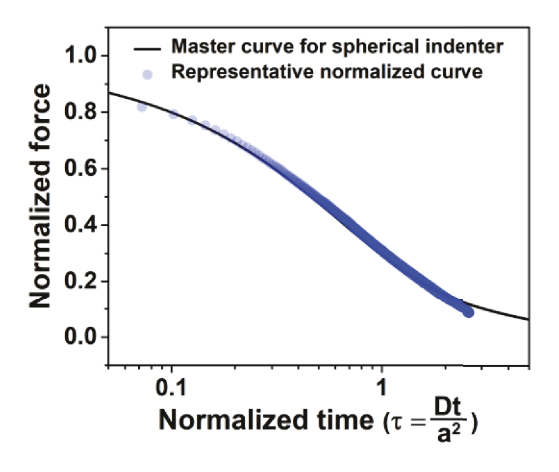


Figure 4 Representative of fitting normalized force relaxation to master curve for contact between spherical indenter and half-space poroelastic material (Hu et al., 2010). The R-squared values for all of the fits were 0.97  $\pm$  0.01.

Weight and thickness of cartilage dramatically decreased during dehydration (Figure 5). The decrease rate of weight was relatively high until about 1.5 hours, gradually slowed down, and became steady after about 4 hours. Weight of dehydrated cartilage at steady state was about 0.25 times that of hydrated cartilage at the beginning. The decrease rate of thickness showed a trend similar to that of weight. It was relatively high in the beginning, and progressively reached steady state. Thickness of dehydrated cartilage at steady state was about 0.3 times that of hydrated cartilage at the beginning. The slight fluctuation of thickness after 4 hours was due to the effect of edge curl on the measurement.

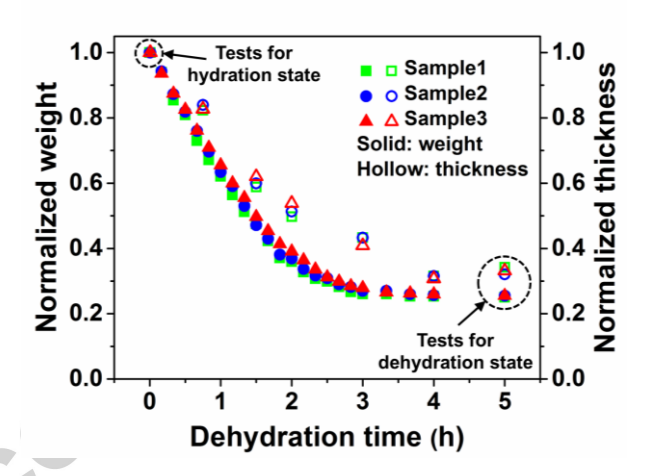


Figure 5 Change in weight and thickness of cartilage during dehydration.

### 4. Discussion

Intrinsic viscoelasticity provided baseline of dissipation over the broadband frequency, and poroelasticity additionally increased overall dissipation (Figure 3a and Figure 6). Phase shifts from  $a_{small}$  and large contact radii (i.e.,  $a_{medium}$  and  $a_{large}$ ) originate from poroviscoelastic dissipation and intrinsic viscoelastic dominant dissipation, respectively (Figure 3a). Therefore, the difference between phase shifts with  $a_{small}$  and  $a_{medium}$  was from the contribution of poroelasticity-driven dissipation; assuming that poroelastic and viscoelastic time constants are

sufficiently different at these contact radii, simple superposition of dissipative effects due to each mechanism is a reliable approximation. The experimentally-measured poroelastic contribution was maximum at 5 Hz in the applied frequency range and  $a_{small}$ , which was consistent with a trend estimated from  $f_{poro}$ 

 $(0.22 \pm 0.09 \text{ Hz})$ . However, the contribution of poroelasticity-driven dissipation at a specific frequency varies depending on a characteristic length (contact radius) (Lai and Hu, 2017; Nia et al., 2011). As the contact radius decreases, the curve of poroelasticity-driven phase shift moves toward a high frequency because  $f_{poro}$  is inversely proportional to the square of a contact radius (Eq. 5) (Lai and Hu, 2017; Nia et al., 2011). For instance, previous work (Nia et al., 2011) showed poroelastic peaks of cartilage at higher frequencies (about 11 Hz) with smaller contact radii (about 6  $\mu$ m) than the current study.

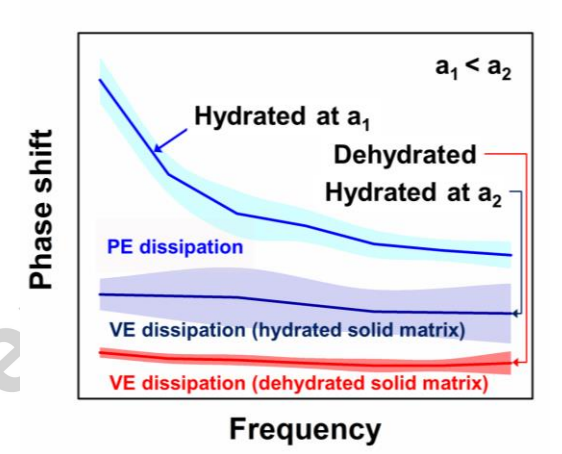


Figure 6 Separation of total energy dissipation into poroelastic, PE, and intrinsic viscoelastic dissipation, VE, over frequency range (5 Hz - 100 Hz). This schematic diagram was plotted based on Figure 3a. Standard deviation was connected using the modified Bezier curve. Intrinsic viscoelasticity provides baseline of dissipation, and poroelasticity additionally increases overall dissipation. Dehydration decreases intrinsic viscoelastic dissipation.

Hydrated cartilage dissipated energy predominantly via molecular friction and rearrangement of the solid matrix (intrinsic viscoelasticity (Nia et al., 2011; Nia et al., 2015)) at large contact radii (i.e.,  $a_{medium}$  and  $a_{large}$ ). The independence of phase shift on contact radius

showed that phase shifts at  $a_{medium}$  and  $a_{large}$  were predominantly from intrinsic viscoelasticity (Figure 3a). In addition, the steady trend of phase shift over the frequency range (5 Hz – 100 Hz) was consistent with previous studies that report macroscale compression and microscale shear results (about 5-14 degrees (Buckley et al., 2013; Fulcher et al., 2009; Lawless et al., 2017)). Since  $\tau_{poro}$  is proportional to the square of contact radius (Eq. 5), poroelastic dissipation is most likely to be suppressed under macroscale compression. Some discrepancies in numerical values could be attributed to various factors: species, age, and test conditions (i.e., full-thickness and induced stress). Consequently,  $a_{medium}$  was large enough to restrict interstitial fluid flow within the applied frequency range, and therefore phase shift at  $a_{medium}$  was predominantly from intrinsic viscoelasticity. This finding demonstrated that broadband intrinsic properties of cartilage can be measured at microscale characteristic lengths; previous studies were limited to macroscale characteristic lengths.

Hydrated cartilage dissipated energy through poroelasticity (solid-fluid frictional interaction (Nia et al., 2011; Nia et al., 2013)) as well as intrinsic viscoelasticity at  $a_{small}$ . Significant difference in phase shifts between  $a_{small}$  and large contact radii (i.e.,  $a_{medium}$  and  $a_{large}$ ) showed additional dissipated energy through poroelasticity at  $a_{small}$  (Figure 3a). Also, the frequency-dependence of phase shift measured at  $a_{small}$  was consistent with the theoretical poroelastic peak,  $f_{poro}$  (0.22  $\pm$  0.09 Hz); it increased toward the peak frequency. D ((3.89  $\pm$  1.64)  $\times$  10<sup>-11</sup> m<sup>2</sup>/s), used for the estimation of  $f_{poro}$ , was consistent with previous studies that used different measurement methods (1.97 $\times$  10<sup>-11</sup> m<sup>2</sup>/s (Lee et al., 2011), 2.30 $\times$  10<sup>-11</sup> m<sup>2</sup>/s (Leddy et al., 2008), and 8.35 $\times$  10<sup>-10</sup> m<sup>2</sup>/s (Aoki et al., 2012)); some discrepancies could be due to samples and strain dependency of D (Greene et al., 2010; Lai et al., 1981). However, the overall consistency of values of D indicates that the simplifying assumption of isotropy is reasonable for this study. The gradual decrease of phase shift over about two decades was also consistent with previous studies that reported poroelasticity-driven phase shift of cartilage (Nia et

al., 2011; Nia et al., 2013). Therefore, phase shift of cartilage at  $a_{small}$  was dominantly from poroelasticity.

Normalizing the frequency with the square of contact radius reiterates the viscoelastic (a<sub>medium</sub> and a<sub>large</sub>) and combined poroviscoelatic (a<sub>small</sub>) dissipation regimes (Lai and Hu, 2017). In the normalized frequency domain, the phase shifts at different contact radii formed united curves (Figure 7). Both the phase shift and the normalized frequency range were consistent with previous macroscale tests (about 10 degrees at 6.76×10<sup>-5</sup> - 5.95×10<sup>-5</sup>10<sup>-3</sup> m²/s (Lawless et al., 2017)). While most data points were along a united curve, the phase shift from a<sub>medium</sub> at low frequency (f=5Hz, a²f= 5.37×10<sup>-9</sup> m²/s) deviated from the overall trend. This was likely due to contact radius decreasing poroelastic dissipation, which was previously observed in biological tissues (Connizzo and Grodzinsky, 2017; Nia et al., 2011; Oftadeh et al., 2018). Combined with the consistency with phase shifts measured at similar frequencies via small magnitude shear loading (about 10 degrees at 0.01, 0.1, and 1 Hz (Buckley et al., 2013)), this suggests predominantly viscoelastic dissipation for a<sub>medium</sub> at low frequency.

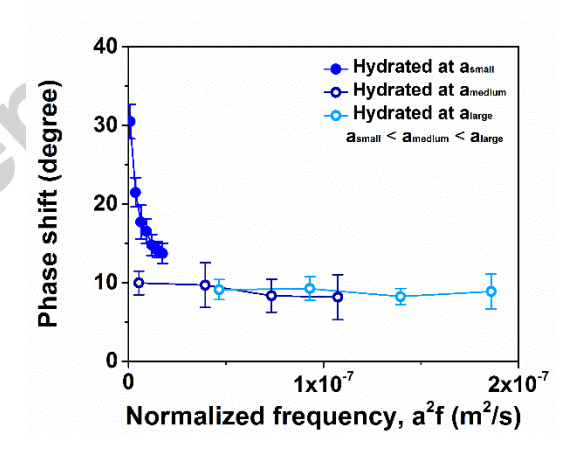


Figure 7 Phase shift curves as function of normalized frequency. The frequency was normalized with the squared of contact radius.

Cartilage exhibited superior energy dissipation compared to isotropic poroelastic materials (e.g., gel); the uncoupled dissipation mechanisms provided reasons of the superiority (Figure 3a,

Figure 6). A previous paper reported the analytical solution of phase shift for dynamic indentation on an isotropic poroelastic material, and verified it by performing dynamic testing on gel with a 25 µm diameter tip (Lai and Hu, 2017). The analytical solution shows that the maximum phase shift from the contact of a sphere with a half-space poroelastic material is about 12 degrees at the poroelastic peak frequency. It is much lower than the maximum phase shift of cartilage measured in this current study  $(30.50 \pm 2.19)$  degrees at 5 Hz). The current finding revealed that intrinsic viscoelasticity of cartilage provided the baseline of about 9 degree phase shift over the frequency range (Figure 3a). Even if the contribution of intrinsic viscoelastic dissipation was excluded, the poroelasticity-driven phase shift of cartilage, which was between phase shifts between a<sub>small</sub> and a<sub>medium</sub> (approximately 20 degrees at 5 Hz), was still higher than the maximum value of an isotropic porous material (12 degrees) (Lai and Hu, 2017). This could be due to the effect of fiber-reinforced structure (Nia et al., 2011) and anisotropy (Mow et al., 1992) of cartilage on poroelasticity-driven dissipation. The anisotropy of collagen fibrils could affect dissipation as they direct fluid flow (Federico and Herzog, 2008, p. aniso); the degree of the anisotropy is expected to be relatively minor when considering the sample age (5-6 months old) (Gannon et al., 2015).

Fluid pressurization was likely the driving factor behind the dependence of dynamic modulus on contact radius. The dependence of overall dynamic modulus on contact radius (Figure 3b) could be due to the degree of interstitial fluid pressurization over the frequency range, evidenced by the uncoupled dominant mechanisms and previous studies. While poroelasticity was dominant at  $a_{small}$ , it was suppressed at large contact radii (i.e.,  $a_{medium}$  and  $a_{large}$ ). Poroelasticity is volumetric effect, so this suggests that cartilage deformed isochorically at large contact radii (i.e.,  $a_{medium}$  and  $a_{large}$ ). Also, the Peclet number ( $\propto \tau_{poro}$  at the same loading rate (Quinn et al., 2001)), a measure of fluid pressurization (Bonnevie et al., 2012; Caligaris and Ateshian, 2008; Quinn et al., 2001), is much higher at a large contact radius (i.e.,  $a_{medium}$  and  $a_{large}$ ) compared to  $a_{small}$ . Therefore, fluid pressurization at a large contact radius (i.e.,  $a_{medium}$  and  $a_{large}$ ) can be inferred to be

higher than that at a<sub>small</sub> in the corresponding frequency (i.e. loading rate) (Caligaris and Ateshian, 2008; Nia et al., 2011; Quinn et al., 2001; Nia et al., 2015). The higher fluid pressure was likely to cause relatively high tensile strain of nonlinear solid matrix (Cohen et al., 1998), resulting in higher dynamic modulus at a large contact radius (i.e.,  $a_{medium}$  and  $a_{large}$ ). The values of dynamic modulus at a large contact radius (i.e.,  $a_{\text{medium}}$  and  $a_{\text{large}}$ ) were consistent with previous studies at macroscale (Fulcher et al., 2009; Lawless et al., 2017). Some discrepancies could be attributed to species and test conditions (i.e., scale and compressive stress). The dependence of self-stiffening of cartilage on contact radius (Figure 3b) was likely due to the effect of frequency on fluid pressurization, underpinned by the determined dominant mechanisms and previous studies (Nia et al., 2011; Nia et al., 2015). The self-stiffening is defined here as the ratio of dynamic moduli at 100 Hz and 5 Hz, and a<sub>small</sub> (about 2.05) exhibited a higher ratio than a<sub>medium</sub> (about 1.25). Phase shift at a<sub>small</sub> showed that poroelastic effect decreased toward 100 Hz, resulted from a relative increase of loading rate in the same poroelastic diffusion time (Caligaris and Ateshian, 2008; Nia et al., 2011; Nia et al., 2015). As a result, interstitial fluid pressure likely increased with frequency, and thus dynamic modulus at a<sub>small</sub> gradually increased (Caligaris and Ateshian, 2008; Nia et al., 2011; Nia et al., 2015). Note that a<sub>small</sub> at 100 Hz was not incompressible because phase shift at a<sub>small</sub> was higher than that at a<sub>medium</sub>, indicating some poroelastic effect. In contrast, in the case of a<sub>medium</sub>, cartilage was virtually incompressible (isochoric deformation) over the frequency range. Consequently, fluid pressurization was relatively steady with frequency, and therefore dynamic modulus was almost constant (Nia et al., 2015). It was consistent with steady trends of dynamic moduli at macroscale from previous studies (Fulcher et al., 2009; Lawless et al., 2017). The slight self-stiffening at a<sub>medium</sub> could be attributed to intrinsic viscoelasticity of solid matrix.

Dehydration dramatically decreased water content and thickness of cartilage (Figure 5). Weight of total water in cartilage is about 60 – 85 % of its wet weight and about 30 % of the total water belongs to intrafibrillar space (Maroudas et al., 1991; Mow et al., 1992; Torzilli, 1985). Therefore, 25 % of the initial cartilage weight at the dehydration state indicated that cartilage lost

substantial water in extrafibriliar and intrafibriliar spaces. Similar to weight, the considerable decrease in thickness was also due to loss of water in extrafibriliar and intrafibriliar spaces. The dramatic change in water content and thickness by air dehydration were consistent with previous studies (e.g., cartilage (Boettcher et al., 2016) and type I collagen (Andriotis et al., 2015)).

Such extreme dehydration had a pronounced effect on phase shift and dynamic modulus of cartilage over the frequency range studied (Figure 3 and Figure 6). Poroelasticity-driven dissipation did not arise due to substantial loss of fluid, evidenced by the disappearance of a poroelastic peak trend in phase shift. A decrease in intrinsic viscoelasticity was most likely due to loss of interfibrillar fluid and increased density of solid matrix (similar to foam materials). This is supported by previous studies on individual collagen fibrils and polymeric structural foams: energy dissipation of Type I collagen fibrils decreased with a progressive dehydration (Uhlig and Magerle, 2017) and density of foams influenced on their absorbed energy (Avalle et al., 2001). This finding suggested that a decreased ability of cartilage to sustain fluid in disease could decrease energy dissipation under dynamic loading conditions in vivo. In addition to affecting energy dissipation, dehydration sharply increased dynamic modulus (Figure 3b). It was likely due to the compaction of cartilage by dehydration, resulting from collapsed pore space and shrinkage of the solid matrix. It could be inferred from the huge decrease in thickness after dehydration. A previous study on Type 1 collagen fibrils provided evidence on shrinkage of fibrils during dehydration (Andriotis et al., 2015). The increase in dynamic modulus was consistent with previous studies that showed fibrils (Andriotis et al., 2015; Wenger et al., 2007) and cartilage (Boettcher et al., 2016) became stiffer after dehydration through quasi-static tests. This finding implies that a decreased ability of the solid matrix to maintain fluid due to disease could affect poroelasticity-driven dissipation over the frequency range of interest because increased stiffness of solid matrix decreases volumetric deformation under the same stress level; poroelasticy-driven dissipation originates from solid-fluid frictional interaction, and fluid flow is related to volumetric deformation (Lakes, 2009).

It is worthwhile to discuss a few limitations of this study. Although the applied frequency (5-100 Hz) covered most of daily activity-induced frequencies (timescales) (Nia et al., 2011) (e.g., walking: 1-8Hz (Cross, 1999), running: 4-100 Hz (Dickinson et al., 1985), kicking: 4-11Hz (Tanaka et al., 2006), and jumping: 2-100 Hz (Richards et al., 1996)), a low frequency range (< 5 Hz) was not covered. It was scarified due to limitations in the data acquisition point coupled with the duration for equilibrium. Nevertheless, the trend of phase shift (5-100 Hz) matched well with that inferred from the expected peak at  $f_{poro}$ . The testing conditions employed in this study are not the same as vivo conditions (e.g., full-thickness); however, they provided information on isolated properties of cartilage (i.e., superficial zone), which enabled uncoupling poroelastic and intrinsic viscoelastic dissipation. The dehydration process was conducted in ambient conditions under controlled humidity. Although the weight and thickness of cartilage was considerably reduced after 5 hours of dehydration, fully-dry cartilage matrix conditions cannot be ensured as the hydration level of cartilage should equilibrate with the ambient humidity. Fully-dry cartilage matrix could be obtained by controlled drying processes such as freeze-drying (Polak and Pitombo, 2011; Taylor, 1945).

In our view, this study provided useful information for cartilage-like dampers (Boz and Eriten, 2018; Liu et al., 2017) and showed a possibility that the current approach could be used to investigate early osteoarthritic damage (Hollander et al., 1995). The uncoupled poroelastic and intrinsic viscoelasticity of cartilage suggested that cartilage-like dampers with efficient and sustained dissipation could be designed by inducing poroelasticity-driven dissipation in addition to intrinsic viscoelasticity-driven dissipation. The current study combined with previous studies (Liu et al., 2017; Nia et al., 2011) suggested dissipation of cartilage-like dampers at a specific frequency can be maximized by utilizing the dependence of  $f_{poro}$  on a characteristic length and diffusivity. In addition, it was demonstrated that poroelastic and intrinsic viscoelastic-dominant properties of superficial zone can be measured at microscale characteristic lengths. This approach

could be useful to investigate early osteoarthritis, initiating from superficial zone (Hollander et al., 1995; Mow et al., 1992).

### 5. Conclusions

In this study, dissipative properties due to poroelasticity and intrinsic viscoelasticity of cartilage were investigated over physiological loading frequencies. Uncoupling between poroelasticity and intrinsic viscoelasticity was achieved via dependence of poroelastic relaxation on characteristic lengths (contact radii in dynamic indentation tests). The uncoupled dissipation mechanisms provided novel information on origins of efficient and sustained broadband dissipation of cartilage; intrinsic viscoelasticity provides baseline of dissipation, and poroelasticity additionally increases overall dissipation. The confirmation of intrinsic viscoelasticity broke the existing broadband test scale of intrinsic properties, limited to macroscale length, and provided a possibility to measure poroelastic (flow-dependent) and intrinsic viscoelastic (flow-independent) properties of cartilage at similar microscale lengths. The decreased dissipation of cartilage following dehydration highlighted the importance of hydration in both poroelasticity and intrinsic viscoelasticity-related losses. The findings extended the current understanding in dynamic dissipative and mechanical properties of cartilage. Promising aspects of cartilage as efficient and sustained dampers were experimentally confirmed, and the findings could be useful to design them as suggested elsewhere (Boz and Eriten, 2018; Liu et al., 2017).

### Acknowledgment

Funding from the National Science Foundation (CMMI-DCSD-1662456) is gratefully acknowledged. The authors are grateful to Shannon K. Walsh and Sunjung Kim for helpful discussions on statistical analysis.

### References

- Andriotis, O.G., Chang, S.W., Vanleene, M., Howarth, P.H., Davies, D.E., Shefelbine, S.J., Buehler, M.J., Thurner, P.J., 2015. Structure–mechanics relationships of collagen fibrils in the osteogenesis imperfecta mouse model. J. R. Soc. Interface 12, 20150701. https://doi.org/10.1098/rsif.2015.0701
- Aoki, T., Watanabe, A., Nitta, N., Numano, T., Fukushi, M., Niitsu, M., 2012. Correlation between apparent diffusion coefficient and viscoelasticity of articular cartilage in a porcine model. Skeletal Radiol. 41, 1087–1092. https://doi.org/10.1007/s00256-011-1340-y
- Avalle, M., Belingardi, G., Montanini, R., 2001. Characterization of polymeric structural foams under compressive impact loading by means of energy-absorption diagram. Int. J. Impact Eng. 25, 455–472. https://doi.org/10.1016/S0734-743X(00)00060-9
- Boettcher, K., Kienle, S., Nachtsheim, J., Burgkart, R., Hugel, T., Lieleg, O., 2016. The structure and mechanical properties of articular cartilage are highly resilient towards transient dehydration. Acta Biomater. 29, 180–187. https://doi.org/10.1016/j.actbio.2015.09.034
- Bonnevie, E.D., Baro, V.J., Wang, L., Burris, D.L., 2012. Fluid load support during localized indentation of cartilage with a spherical probe. J. Biomech. 45, 1036–1041. https://doi.org/10.1007/s10955-011-0269-9.Quantifying
- Boz, U., Eriten, M., 2018. A numerical investigation of damping in fuzzy oscillators with poroelastic coating attached to a host structure. J. Sound Vib. 417, 277–293. https://doi.org/10.1016/j.jsv.2017.12.008
- Buckley, M.R., Bonassar, L.J., Cohen, I., 2013. Localization of viscous behavior and shear energy dissipation in articular cartilage under dynamic shear loading. J. Biomech. Eng. 135, 31002-1-31002–9. https://doi.org/10.1115/1.4007454
- Caligaris, M., Ateshian, G.A., 2008. Effects of sustained interstitial fluid pressurization under migrating contact area, and boundary lubrication by synovial fluid, on cartilage friction. Osteoarthr. Cartil. OARS Osteoarthr. Res. Soc. 16, 1220–1227. https://doi.org/10.1016/j.joca.2008.02.020
- Cohen, B., Lai, W.M., Mow, V.C., 1998. A transversely isotropic biphasic model for unconfined compression of growth plate and chondroepiphysis. J. Biomech. Eng. 120, 491–496. https://doi.org/10.1115/1.2798019
- Connizzo, B.K., Grodzinsky, A.J., 2017. Tendon exhibits complex poroelastic behavior at the nanoscale as revealed by high-frequency AFM-based rheology. J. Biomech. 54, 11–18. https://doi.org/10.1016/j.jbiomech.2017.01.029
- Cross, R., 1999. Standing, walking, running, and jumping on a force plate. Am. J. Phys. 67, 304. https://doi.org/10.1119/1.19253
- Dickinson, J.A., Cook, S.D., Leinhardt, T.M., 1985. The measurement of shock waves following heel strike while running. J. Biomech. 18, 415–422. https://doi.org/10.1016/0021-9290(85)90276-3
- Federico, S., Herzog, W., 2008. On the anisotropy and inhomogeneity of permeability in articular cartilage. Biomech. Model. Mechanobiol. 7, 367–378. https://doi.org/10.1007/s10237-007-0091-0
- Fulcher, G.R., Hukins, D.W., Shepherd, D.E., 2009. Viscoelastic properties of bovine articular cartilage attached to subchondral bone at high frequencies. BMC Musculoskelet. Disord. 10, 61. https://doi.org/10.1186/1471-2474-10-61
- Gannon, A.R., Nagel, T., Bell, A.P., Avery, N.C., Kelly, D.J., 2015. Postnatal changes to the mechanical properties of articular cartilage are driven by the evolution of its collagen network. Eur. Cell. Mater. 29, 105-121; discussion 121-123.
- Greene, G.W., Zappone, B., Söderman, O., Topgaard, D., Rata, G., Zeng, H., Israelachvili, J.N., 2010. Anisotropic dynamic changes in the pore network structure, fluid diffusion and fluid flow in articular cartilage under compression. Biomaterials 31, 3117–3128. https://doi.org/10.1016/j.biomaterials.2010.01.102

- Henak, C.R., Ross, K.A., Bonnevie, E.D., Fortier, L.A., Cohen, I., Kennedy, J.G., Bonassar, L.J., 2016. Human talar and femoral cartilage have distinct mechanical properties near the articular surface. J. Biomech. https://doi.org/http://dx.doi.org/10.1016/j.jbiomech.2016.08.016
- Hertz, H., 1881. On the contact of elastic solids. J. Reine Angew. Math. 92, 156–171.
- Hollander, A.P., Pidoux, I., Reiner, A., Rorabeck, C., Bourne, R., Poole, A.R., 1995. Damage to type II collagen in aging and osteoarthritis starts at the articular surface, originates around chondrocytes, and extends into the cartilage with progressive degeneration. J. Clin. Invest. 96, 2859–2869. https://doi.org/10.1172/JCI118357
- Hu, Y., Zhao, X., Vlassak, J.J., Suo, Z., 2010. Using indentation to characterize the poroelasticity of gels. Appl. Phys. Lett. 96. https://doi.org/10.1063/1.3370354
- Hysitron, I., 2014. TriboIndenter nanoDMA<sup>TM</sup> User Manual.
- June, R.K., Ly, S., Fyhrie, D.P., 2009. Cartilage stress-relaxation proceeds slower at higher compressive strains. Arch. Biochem. Biophys. 483, 75–80. https://doi.org/10.1016/j.abb.2008.11.029
- Lai, W.M., Mow, V.C., Roth, V., 1981. Effects of nonlinear strain-dependent permeability and rate of compression on the stress behavior of articular cartilage. J. Biomech. Eng. 103, 61–66. https://doi.org/10.1115/1.3138261
- Lai, Y., Hu, Y., 2017. Unified solution for poroelastic oscillation indentation on gels for spherical, conical and cylindrical indenters. Soft Matter 13, 852–861. https://doi.org/10.1039/C6SM02341J
- Lakes, P.R., 2009. Viscoelastic Materials, 1 edition. ed. Cambridge University Press, Cambridge; New York.
- Lawless, B.M., Sadeghi, H., Temple, D.K., Dhaliwal, H., Espino, D.M., Hukins, D.W.L., 2017. Viscoelasticity of articular cartilage: Analysing the effect of induced stress and the restraint of bone in a dynamic environment. J. Mech. Behav. Biomed. Mater. 75, 293–301. https://doi.org/10.1016/j.jmbbm.2017.07.040
- Leddy, H.A., Christensen, S.E., Guilak, F., 2008. Microscale diffusion properties of the cartilage pericellular matrix measured using 3D scanning microphotolysis. J. Biomech. Eng. 130, 061002-061002-8. https://doi.org/10.1115/1.2979876
- Lee, J.I., Sato, M., Ushida, K., Mochida, J., 2011. Measurement of diffusion in articular cartilage using fluorescence correlation spectroscopy. BMC Biotechnol. 11, 19. https://doi.org/10.1186/1472-6750-11-19
- Liu, L., Usta, A.D., Eriten, M., 2017. A broadband damper design inspired by cartilage-like relaxation mechanisms. J. Sound Vib. 406, 1–14. https://doi.org/10.1016/j.jsv.2017.06.010
- Mak, A.F., 1986. The apparent viscoelastic behavior of articular cartilage—the contributions from the intrinsic matrix viscoelasticity and interstitial fluid flows. J. Biomech. Eng. 108, 123–130. https://doi.org/10.1115/1.3138591
- Maroudas, A., Wachtel, E., Grushko, G., Katz, E.P., Weinberg, P., 1991. The effect of osmotic and mechanical pressures on water partitioning in articular cartilage. Biochim. Biophys. Acta BBA Gen. Subj. 1073, 285–294. https://doi.org/10.1016/0304-4165(91)90133-2
- Mow, V.C., Ratcliffe, A., Robin Poole, A., 1992. Cartilage and diarthrodial joints as paradigms for hierarchical materials and structures. Biomaterials 13, 67–97. https://doi.org/10.1016/0142-9612(92)90001-5
- Nia, H., Han, L., Li, Y., Ortiz, C., Grodzinsky, A., 2011. Poroelasticity of cartilage at the nanoscale. Biophys. J. 101, 2304–2313. https://doi.org/10.1016/j.bpj.2011.09.011
- Nia, H., Bozchalooi, I.S., Li, Y., Han, L., Hung, H.H., Frank, E., Youcef-Toumi, K., Ortiz, C., Grodzinsky, A., 2013. High-Bandwidth AFM-based rheology reveals that cartilage is most sensitive to high loading rates at early stages of impairment. Biophys. J. 104, 1529–1537. https://doi.org/10.1016/j.bpj.2013.02.048

- Nia, H., Han, L., Soltani Bozchalooi, I., Roughley, P., Youcef-Toumi, K., Grodzinsky, A.J., Ortiz, C., 2015. Aggrecan nanoscale solid–fluid interactions are a primary determinant of cartilage dynamic mechanical properties. ACS Nano 9, 2614–2625. https://doi.org/10.1021/nn5062707
- Oftadeh, R., Connizzo, B.K., Nia, H.T., Ortiz, C., Grodzinsky, A.J., 2018. Biological connective tissues exhibit viscoelastic and poroelastic behavior at different frequency regimes: Application to tendon and skin biophysics. Acta Biomater. https://doi.org/10.1016/j.actbio.2018.01.041
- Polak, R., Pitombo, R.N.M., 2011. Care during freeze-drying of bovine pericardium tissue to be used as a biomaterial: A comparative study. Cryobiology 63, 61–66. https://doi.org/10.1016/j.cryobiol.2011.05.001
- Quinn, T.M., Allen, R.G., Schalet, B.J., Perumbuli, P., Hunziker, E.B., 2001. Matrix and cell injury due to sub-impact loading of adult bovine articular cartilage explants: Effects of strain rate and peak stress. J. Orthop. Res. 19, 242–249. https://doi.org/10.1016/S0736-0266(00)00025-5
- Richards, D.P., Ajemian, S. V., Wiley, J.P., Zernicke, R.F., 1996. Knee joint dynamics predict patellar tendinitis in elite volleyball players. Am. J. Sports Med. 24, 676–683. https://doi.org/10.1177/036354659602400520
- Tanaka, Y., Shiokawa, M., Yamashita, H., Tsuji, T., 2006. Manipulability analysis of kicking motion in soccer based on human physical properties, in: 2006 IEEE International Conference on Systems, Man and Cybernetics. pp. 68–73. https://doi.org/10.1109/ICSMC.2006.384360
- Taylor, A.C., 1945. The rates of freezing, drying and rehydration of nerves. J. Cell. Comp. Physiol. 25, 161–173. https://doi.org/10.1002/jcp.1030250302
- Torzilli, P.A., 1985. Influence of cartilage conformation on its equilibrium water partition. J. Orthop. Res. 3, 473–483. https://doi.org/10.1002/jor.1100030410
- Uhlig, M.R., Magerle, R., 2017. Unraveling capillary interaction and viscoelastic response in atomic force microscopy of hydrated collagen fibrils. Nanoscale 9, 1244–1256. https://doi.org/10.1039/C6NR07697A
- Wenger, M.P.E., Bozec, L., Horton, M.A., Mesquida, P., 2007. Mechanical properties of collagen fibrils. Biophys. J. 93, 1255–1263. https://doi.org/10.1529/biophysj.106.103192

# Highlights

- The relative contributions of poroelasticy and intrinsic viscoelasticity were decoupled over physiological loading frequencies.
- Intrinsic viscoelasticity provided baseline of broadband dissipation, and poroelasticity additionally increased overall dissipation.
- Cartilage exhibited superior energy dissipation compared to isotropic poroelastic materials (e.g., gel).
- Substantial loss of fluid decreased intrinsic viscoelasticity.
- Both poroelastic (flow-dependent) and intrinsic viscoelastic (flow-independent) properties of cartilage were measured at similar microscale lengths.